Thermochronometric and textural evidence for seismicity via asperity flash heating on exhumed hematite fault mirrors, Wasatch fault zone, UT, USA

Robert G. McDermott [a,*], Alexis K. Ault [a], James P. Evans [a], Peter W. Reiners [b]

[a] *Department of Geology, Utah State University, 4505 Old Main Hill, Logan, UT 84322, USA*
[b] *Department of Geosciences, University of Arizona, 1040 E. 4th St., Tucson, AZ 85721, USA*

ABSTRACT

Exhumed faults record the temperatures produced by earthquakes. We show that transient elevated fault surface temperatures preserved in the rock record are quantifiable through microtextural analysis, fault-rock thermochronometry, and thermomechanical modeling. We apply this approach to a network of mirrored, minor, hematite-coated fault surfaces in the exhumed, seismogenic Wasatch fault zone, UT, USA. Polygonal and lobate hematite crystal morphologies, coupled with hematite (U–Th)/He data patterns from these surfaces and host rock apatite (U–Th)/He data, are best explained by friction-generated heat at slip interface geometric asperities. These observations inform thermomechanical simulations of flash heating at frictional contacts and resulting fractional He loss over generated fault surface time–temperature histories. Temperatures of $> \sim 700$–$1200\,^\circ C$, depending on asperity size, are sufficient to induce 85–100% He loss from hematite within 200 μm of the fault surface. Spatially-isolated, high-temperature microtextures imply spatially-variable heat generation and decay. Our results reveal that flash heating of asperities and associated frictional weakening likely promote small earthquakes ($M_w \approx -3$ to 3) on Wasatch hematite fault mirrors. We suggest that similar thermal processes and resultant dynamic weakening may facilitate larger earthquakes.

© 2017 Elsevier B.V. All rights reserved.

1. Introduction

Friction-generated heat is a primary by-product of seismicity (Sibson, 1975; Spray, 1992; Rowe and Griffith, 2015 and references therein). Heat is a first-order control on the physical mechanisms behind coseismic fault strength reduction, which is a prerequisite for earthquake nucleation and propagation (Brace and Byerlee, 1966; Scholz, 1998). Fault surface paleothermometers (e.g., Sibson, 1975; Polissar et al., 2011; Rowe and Griffith, 2015) can be used to estimate coseismic shear stress, a key variable in understanding dynamic rupture and slip (Brace and Byerlee, 1966; Zheng and Rice, 1998; Lapusta and Rice, 2003), earthquake energy budgets (Kanamori and Rivera, 2006), and recurrence intervals (Dieterich and Kilgore, 1996). *In situ* documentation and quantification of fault paleotemperatures are critical to deciphering the rock record of earthquakes and understanding the physics of earthquake processes at all scales.

Mineral coatings on slip surfaces preserve nano- to microscale deformation textures that reflect coseismic temperature and strength changes. For example, relict silica colloids on natural, silica-rich slip surfaces suggest gel lubrication as a weakening mechanism (Kirkpatrick et al., 2013). Amorphous Ca-oxide on carbonate faults imply decarbonation and concomitant weakening from elevated coseismic temperatures (Collettini et al., 2013). These observations complement rotary shear experiments illustrating thermally activated lubrication or flash heating-induced low frictional strength (e.g., Hirose and Bystricky, 2007; Goldsby and Tullis, 2011; Di Toro et al., 2011 and references therein). The diverse lithologic makeup of natural fault zones merits investigation of the signatures of earthquake processes in other mineral phases. Hematite is commonly found on fault surfaces and may record thermomechanical information related to the seismic cycle.

Hematite is amenable to (U–Th)/He (He) thermochronometry, and we use this method to detect elevated paleotemperatures from past earthquakes on *mirrored* or high gloss, light reflective hematite-coated fault surfaces from Wasatch fault zone (WFZ), northern Utah. The diffusion of He from hematite, and thus hematite He dates, respond to short-duration, high-temperature,

localized thermal anomalies that characterize fault slip (Ault et al., 2015). Prior geochemical, microtextural, and thermochronologic study of some WFZ hematite slip surfaces suggest they may record elevated fault surface temperatures (Evans et al., 2014; Ault et al., 2015). We present 114 new and published (Ault et al., 2015) individual hematite He dates and new apatite He data. A subset of hematite aliquots were prescreened with scanning electron microscopy (SEM) prior to (U–Th)/He analysis to link texture development with thermochronometry data patterns. We then parameterize models of flash heating at asperities, or frictional contacts, with attendant hematite He loss using microtextural and thermochronometric observables to determine if this dynamic weakening mechanism can explain our results. Modeled temperature rise at asperities is consistent with our data patterns, suggesting this process potentially promotes seismicity on these fault mirrors.

2. Hematite (U–Th)/He thermochronometry of fault rocks

Hematite He dates from hematite-coated fault surfaces reflect the thermal and mechanical processes operative within fault systems. Retention of radiogenic He in polycrystalline hematite depends on the distribution of individual diffusion domains, temperature, and cooling rate (Farley and Flowers, 2012; Evenson et al., 2014). The temperature transition from open to closed system behavior, or onset of He retention – the closure temperature, T_c (Dodson, 1973), is between ~25–250 °C in the hematite He system (Farley and Flowers, 2012; Evenson et al., 2014). Individual crystallites are inferred to be the He diffusion domains and T_c increases with grain (domain) size (Evenson et al., 2014). Variations in bulk T_c are controlled by the grain size distribution in each polycrystalline aliquot.

Hematite mineralization occurs over a range of depths within the Earth that correspond to ambient temperatures either below or above its T_c, given an initial grain size distribution. If hematite forms and remains below its T_c (i.e., lower T, shallower depth), hematite He data record the timing of hematite formation (Ault et al., 2015, 2016). Alternatively, hematite may form at greater depths with higher ambient temperatures than its T_c. Subsequent cooling to below the hematite He T_c via exhumation yields a He date that reflects this cooling history (Farley and Flowers, 2012; Evenson et al., 2014). Hematite on fault surfaces experience heat and/or strain associated with fault slip. Mechanical grain size reduction during cataclasis can progressively lower the T_c. If fault surface hematite accumulates He below its T_c, thermal pulses from fault slip induce He loss from the crystal lattice by volume diffusion and/or recrystallization (Ault et al., 2015). Circulation of hot fluids along faults may also reset He dates (Ault et al., 2016). Under these nonmonotonic cooling scenarios, the temperatures required for appreciable He loss are inversely proportional to the duration of heating (Fechtig and Kalbitzer, 1966; Reiners, 2009; Ault et al., 2015). If the timescale of heating is only a few seconds to minutes, requisite temperatures for He loss and resetting of the He date must substantially exceed the T_c.

Interpreting fault surface hematite He dates requires information on the hematite mineralization age, microtextural characterization, grain size (and therefore T_c) measurements, and independent constraints on the ambient cooling history. Here, we acquire hematite He dates from specular veins, a potential precursor to the fault mirror hematite (Evans and Langrock, 1994; Ault et al., 2015). We characterize fault surface microtextures and aliquot grain size distributions with SEM to identify evidence of heat and deformation on these surfaces and bracket the aliquot T_c. We use apatite (U–Th)/He thermochronometry to track cooling of the WFZ footwall. The apatite He system is sensitive to temperatures of ~30–90 °C, depending on the accumulation and annealing
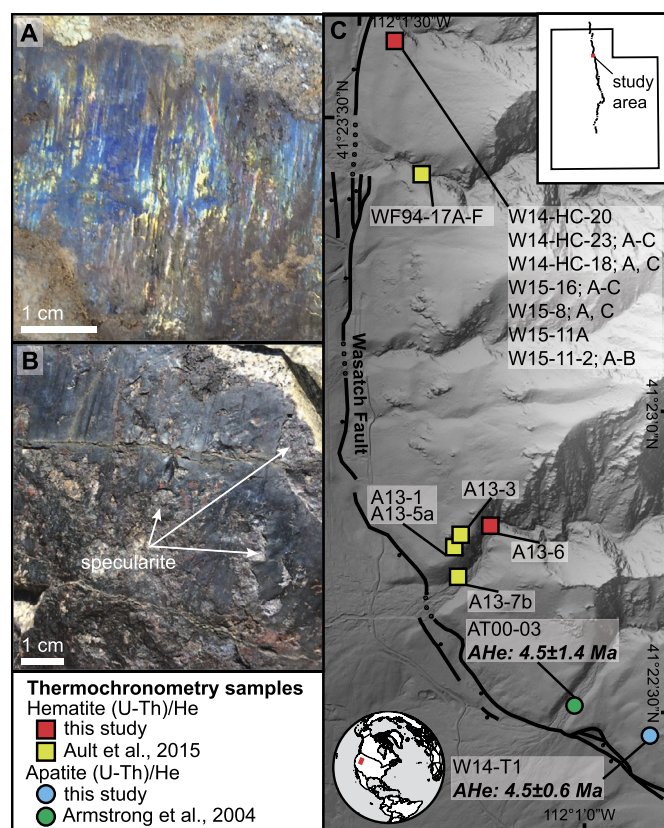

Fig. 1. Hematite fault surfaces, sample localities, and apatite (U–Th)/He dates for the Wasatch Fault zone, UT. (A, B) Field photographs of high-gloss, hematite-coated minor faults with local iridescence and slickenlines (A) and specular hematite below fault surface (B). (C) Southern Brigham City segment of WFZ. Red and yellow squares are hematite sample locations in this study and from Ault et al. (2015). Blue and green circles are apatite He sample locations from this study and Armstrong et al. (2004). Dates reported as mean and 1σ standard deviation. Base map digital elevation model (DEM) is 0.5 m LiDAR from Utah Geological Survey. Quaternary fault scarps (black lines) mapped from DEM. Inset shows extent of WFZ. Red square denotes study area. (For interpretation of the references to color in this figure legend, the reader is referred to the web version of this article.)

of decay-induced radiation damage, thermal history, and crystal size (Flowers et al., 2009). In rapidly cooled settings, such as the footwall of a normal fault, the apatite He T_c is typically ~50–60 °C (10 °C/Ma cooling rate), corresponding to cooling though ~1–3 km depth. Prior study of WFZ fault surfaces report hematite crystallite radii (and thus diffusion domain length scales) of 0.05 to 5 μm, corresponding to a hematite He T_c of ~75–150 °C (10 °C/Ma cooling rate; Ault et al., 2015). Complementary apatite He dates from nearby unaltered bedrock place a lower temporal bound on hematite He dates that record ambient cooling (Ault et al., 2015).

3. Multi-scale characterization of hematite fault mirrors

The WFZ hematite-coated fault surfaces are exposed in a ~300–400 m-thick footwall damage zone in Paleoproterozoic Farmington Canyon Complex gneiss (Fig. 1; Evans et al., 2014). Faults are mirrored, or high-gloss and light reflective. They are arcuate to planar, locally iridescent, ≤2 mm-thick, and commonly have <1–10 cm of observed offset (Figs. 1A, B; Evans and Langrock, 1994; Evans et al., 2014). Slickenlines and tool marks and grooves from asperity ploughing indicate dominantly normal, down-to-the-west slip compatible with WFZ extension and thus likely developed after initiation of the WFZ at ~12 Ma (Evans and Langrock, 1994; Ehlers et al., 2003). Fault surfaces exhibit one to several sets of slickenlines, indicating multiple slip events (Evans and Langrock, 1994; Evans et al., 2014). Samples analyzed in this study are gen-

erally planar and contain one or two visible lineations (Fig. S1). Field and microtextural observations suggest many now mirrored surfaces originated as specular hematite veins later modified by progressive slip and grain comminution (Figs. 1B; S1; Evans and Langrock, 1994; Ault et al., 2015).

We characterize the texture and grain size distribution of hematite aliquots extracted from specularite veins and high-gloss fault surfaces with secondary electron and back-scattered electron SEM imaging. Instrument operating conditions, detailed sample preparation notes, and the grain size measurement approach are described in the Supplementary Material. Hematite aliquots were extracted using a portable rotary tool and fine point tweezers and selected to avoid tool marks. All aliquots are approximately cubic or rectangular in shape with fault-surface-perpendicular widths of ~120–200 μm (Figs. S2; S3). Hematite polycrystalline aggregates representative of dated aliquots were mounted in epoxy, polished in cross-sectional view, and imaged under high vacuum. SEM-prescreened aliquots (10–11 per sample) were mounted on copper sticky tape and imaged under low vacuum. Four to five of these aliquots were then selected for (U–Th)/He analysis to encapsulate a range of observed fault surface microtextures. Aliquots were removed from copper sticky tape mounts and inserted into Nb tubes without manipulation or breakage to preserve documented microtextures.

Vein samples (W14-HC-20, A13-6) comprise euhedral to subhedral, locally fractured, hematite plates with 0.07–10 μm half-widths (Table S1; Fig. S2). Fault surfaces comprise comminuted, subhedral, subrounded to subangular grains with minimum and maximum grain radii/half-widths of 0.02 and 1.5 μm, respectively, although the majority are 0.1–0.5 μm (Table S1). Some fault surfaces contain crystals with polygonal, triple junction-forming (~120°) grain boundaries (Fig. 2A–C) and/or lobate grain boundaries (Fig. 2D–F). These grain morphologies lack shape-preferred orientation and occur in spatially isolated ≤1–20 μm clusters at the slip surface surrounded by lobate and/or subangular grains (Figs. 2; S3; S4).

4. Hematite and apatite (U–Th)/He thermochronometry results

We report 66 new hematite He dates from seven fault surfaces and two veins combined with previously published results (Table S2; Fig. 3A; Ault et al., 2015). Hematite aliquots were analyzed for He, U, and Th at the University of Arizona using standard apatite lasing temperatures to prevent U and Th volatilization and zircon dissolution procedures. Additional details are provided in the Supplementary Material. Mean hematite He dates from high-gloss fault surfaces range from 12.3 ± 4.2 Ma to 2.4 ± 1.0 Ma ($\pm 1\sigma$ standard deviation) with individual aliquot dates spanning 18.4 ± 0.6 Ma to 1.4 ± 0.2 Ma ($\pm 2\sigma$ analytical error). Samples exhibit variable intrasample reproducibility with ~50% of samples yielding <10% sample mean standard deviation. Hematite He dates from undeformed vein samples (W14-HC-20, A13-6) are 88.5 ± 15.2 Ma and 10.7 ± 0.8 Ma. For comparison and to track the ambient fault footwall cooling, we acquired an apatite He date from isoelevational and unaltered host rock gneiss. The apatite He date of 4.5 ± 0.6 Ma overlaps previously published apatite He data from ~300 m to the northwest (method details in the Supplementary Material; Table S3; Fig. 1; Armstrong et al., 2004).

Thermochronometry results exhibit four important patterns. First, fault surface aliquots yield hematite He dates younger than those from specular vein samples W14-HC-20 and A13-6, with the exception of outliers from sample A13-3 (Fig. 3A). Second, 48% of fault surface hematite He dates are younger than the ~4.5 Ma apatite He date (Fig. 3B). Third, hematite He dates from two locations on the same fault surface (W15-16A, C) are internally consistent at <10% 1σ sample mean standard deviation, but distinct

A | D
10 μm | 10 μm
B | E
1 μm | 1 μm
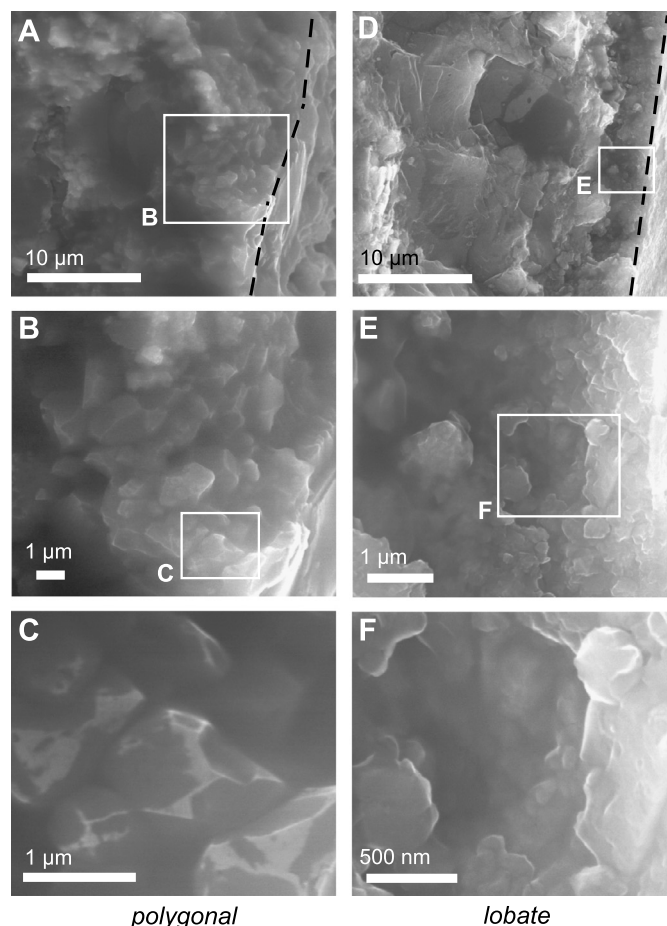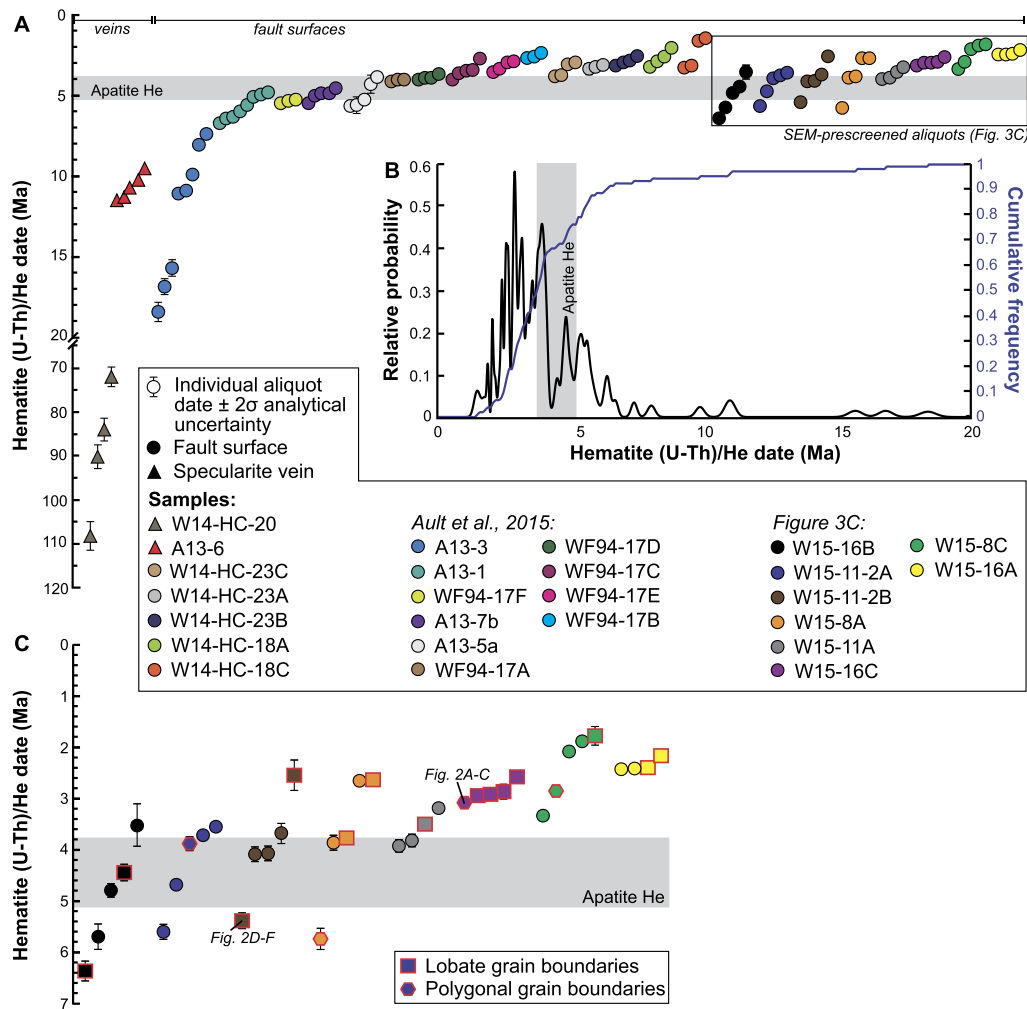C | F
1 μm | 500 nm
polygonal | *lobate*

Fig. 2. Fault surface hematite morphology and microtextures. Scanning electron microscopy (SEM) secondary electron (SE) images at different scales showing examples of hematite with polygonal (A–C; sample W15-16C) and lobate (D–F; W15-11-2B) grain boundaries. Black dashed line denotes fault surface.

(2.3 ± 0.1 Ma and 2.9 ± 0.2 Ma), mirroring previously published data patterns for another fault surface sample (WF94-17A, B, D, E, F; Ault et al., 2015). Finally, for (U–Th)/He-dated prescreened aliquots that purposefully encapsulate the range of crystal morphologies in each sample, aliquots containing clusters of crystals with polygonal or lobate grain boundaries yield hematite He dates that are typically younger than the apatite He data (Fig. 3C). Polygonal and lobate grain morphologies were documented in 18 of 38 pre-screened aliquots. Of these 18 aliquots, 13 (72%) yield dates statistically younger at 1σ standard deviation of our acquired apatite He date, two (12%) overlap the apatite He date, and three (16%) are older than the apatite He date. Hematite He dates from these samples also generally display larger intrasample scatter than results from fault surfaces that were not prescreened, with the exception of samples W15-16A and W15-16C.

5. Evidence for elevated fault surface temperatures

Hematite crystal morphologies and microtextures reveal evidence for elevated fault surface temperatures. The polygonal hematite grain morphology is similar to textures interpreted as recrystallized hematite in previous study of WFZ surfaces (Ault et al., 2015). These morphologies are analogous to that observed in long-duration hematite torsion (Siemes et al., 2003, 2011) and dry heating (Vallina et al., 2014) experiments to 1000–1100 °C. Lobate grains are similar to those observed in torsion and dry heating experiments conducted at lower temperatures (300–800 °C; Siemes et al., 2003, 2011; Vallina et al., 2014). Laboratory and field studies

Fig. 3. Hematite and apatite (U–Th)/He thermochronometry data. (A) Hematite He dates for individual aliquots classified by sample with 2σ analytical error. (B) Relative probability (black line) and cumulative frequency (blue line) of hematite He dates. (C) Subset of SEM-prescreened hematite He dates with complementary microtextural data. Aliquots with polygonal (red hexagon, Fig. 2A–C) and lobate (red square, Fig. 2D–F) grain boundaries highlighted. Gray bar in A, B, and C is new apatite He date (mean ±1σ standard deviation). (For interpretation of the references to color in this figure legend, the reader is referred to the web version of this article.)

of calcite slip surfaces report similar grain morphologies associated with high coseismic strain rates and temperatures (Smith et al., 2013; De Paola et al., 2015). These previous studies suggest such textures are the result of annealing (recrystallization) and/or sintering.

We posit that documented polygonal to lobate hematite grain morphologies from the hematite-coated fault surfaces reflect similar processes. Annealing involves dislocation migration and removal, which require high temperatures but can be facilitated by an applied strain rate. The lack of a shape-preferred grain orientation suggests a component of hematite recrystallization occurred at the low differential stress and strain rate of the "static" post-slip period. On-going annealing under static conditions may have occurred in areas that experienced rapid dislocation migration and high friction-generated temperatures during the coseismic period (e.g., Trepmann et al., 2007). Comparison of our observed microtextures with experimental data indicates paleotemperatures of ≥300–1000 °C at the fault surface.

Thermochronometric data patterns suggest complex and spatially variable fault surface thermal histories. We use T_c calculations as an index of fault surface hematite He retentivity and temperature sensitivity. For this thought experiment, we assume a spherical diffusion length-scale equivalent to the majority of our hematite crystal radii observed with SEM (0.1–0.5 μm), a 10 °C/Ma monotonic cooling rate, and published hematite He diffusion kinet-

ics (Evenson et al., 2014). We compare these data with a calculated host rock apatite He T_c under the same ambient cooling condition and with the approach of Flowers et al. (2009). The apatite He T_c calculation assumes the diffusion kinetics of Flowers et al. (2009), an effective uranium concentration of 30 ppm, and a diffusion domain length-scale of 35 μm (Table S3). The (U–Th)/He T_c estimates for fault surface hematite and host rock apatite are ~95–110 °C (Table S1) and ~55 °C, respectively. Progressive grain size reduction due to fault slip and cataclasis decreases hematite He T_c during footwall exhumation (Ault et al., 2015). Our measured grain size distribution was produced during the most recent slip event and therefore provides minimum T_c estimates. Fault surface hematite He dates younger than the apatite He date are not consistent with hematite He dates recording ambient footwall cooling. Variable hematite He dates from different locations on individual fault surfaces (e.g., W15-16A, C and WF94-17A, B, D, E, F), as well as intrasample date variability for aliquots with similar grain size distributions and thus T_c, further argue against some hematite He dates recording footwall exhumation.

Hematite fault mirrors with high-temperature microtextures that yield hematite He dates younger than the apatite He date provide evidence of (1) past friction-generated heat at the fault surface and (2) attendant thermal resetting (He loss) of the hematite He system. Our T_c calculations and apatite and hematite He date relationships indicate the hematite He system in the WFZ

records these processes at depths shallower than the apatite He T_c isotherm ($\sim\leq 2$ km, assuming a geothermal gradient of 30 °C/km; Blackett, 2004). This does not preclude fault slip events and associated shear heating on these surfaces at greater depths and higher ambient temperatures. Prior faulting caused grain size reduction of specularite veins, decrease in the hematite diffusion domain length scale, and lower T_c, facilitating resetting by subsequent shear heating (Ault et al., 2015). Some samples from the same fault surface comprise aliquots with hematite He dates older and younger than the apatite He date, where both populations display high-temperature microtextures (Fig. 3C). This may be a result of slip events that occurred at ambient temperatures in excess of the apatite He T_c isotherm prior to $\sim$4.5 Ma. The presence of clusters of high-temperature microtextures directly at the slip interface in SEM-prescreened samples, regardless of corresponding hematite He date, argues against this (Figs. 2; S3). Samples with high intrasample hematite He data scatter may be explained by spatially variable He loss. For example, consider hematite with a pre-slip He date of 6.5 Ma (the oldest observed date from surface W15-16) that experienced a slip event at 2.3 Ma (the mean of sample W15-16C). In this hypothetical scenario, $\leq 65\%$ He loss over the scale of a measured aliquot will yield an apparent hematite He date that is older, or falls within, the 4.5 ± 0.6 Ma range of our acquired apatite He date. Thus, the relationships presented in Figure 3C and microtextural context of observed polygonal and lobate grains collectively suggest spatially-variable shear heating at shallow depths and post-4.5 Ma.

An alternative mechanism that could yield hematite He dates younger than apatite He dates is fluid circulation at temperatures below the apatite He T_c isotherm, but this is ruled out based on microtextures and date patterns. Vein hematite He dates are older than fault surface results and suggest multiple generations of vein formation (Fig. 3A). Pervasive comminution in all fault samples and clusters of high-temperature microtextures at the fault surface imply that the most recent events to affect samples were cataclasis followed by localized frictional heating. We observe no textural evidence of neomineralization (i.e., platy hematite growth) overprinting cataclastic and/or recrystallized hematite textures in our aliquots.

6. Thermomechanical modeling of flash heating at geometric asperities

Thermochronometric and microtextural data patterns suggest hematite fault mirrors experienced localized, transient frictional heating from fault slip in the upper 2 km of the crust. The primary controls on friction-generated heat on fault surfaces are the coefficient of friction and normal stress (i.e., shear stress), displacement, slip velocity, and shear zone width (Lachenbruch, 1986). At the fast slip rates that characterize earthquakes (i.e., >0.001 m/s; Rowe and Griffith, 2015), heat production outpaces heat dissipation and shear heating at the slip surface may be high (e.g., Lachenbruch, 1986). Laboratory studies of fault friction indicate a correlation between dynamic fault strength and slip velocity (e.g., Dieterich, 1979; Di Toro et al., 2011 and references therein). At slip rates ≥ 0.1 m/s, thermally-activated weakening mechanisms reduce fault friction and strength (Di Toro et al., 2011). Different dynamic weakening mechanisms inferred from laboratory, theoretical, or field studies reflect effects of lithology, fluid content, and/or the rate of heat production vs. dissipation (e.g., Di Toro et al., 2011 and references therein). These mechanisms include lubrication by the formation of melt (Sibson, 1975; Hirose and Shimamoto, 2005), gels (Kirkpatrick et al., 2013), weak mineral phases at the slip surface (Hirose and Bystricky, 2007), decreases in effective normal stress and/or gouge fluidization by thermal pressurization of pore fluids (Brantut et al., 2008), and weak-
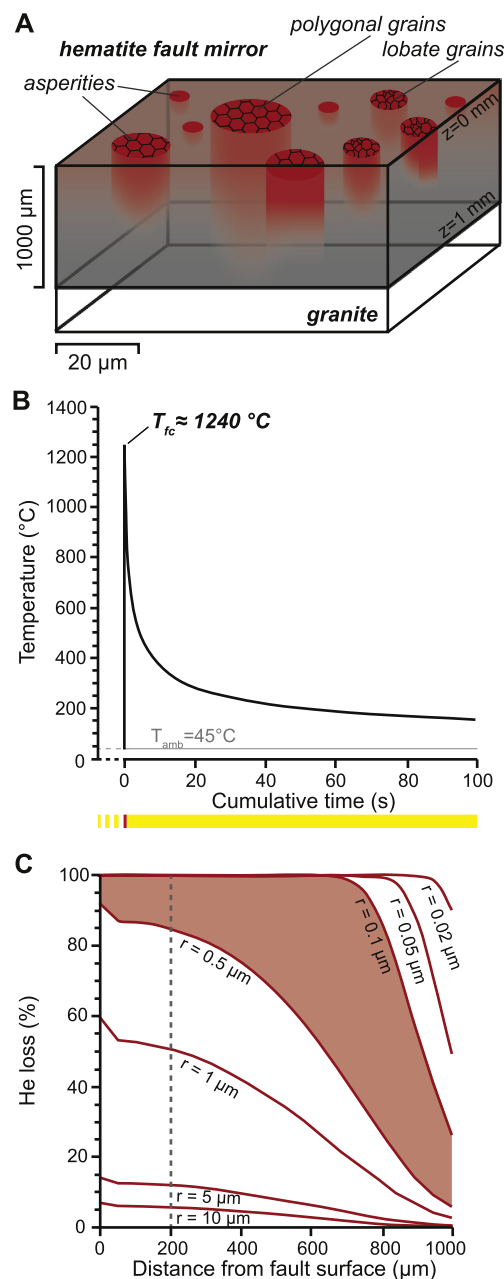
Fig. 4. (A) Schematic of hematite fault mirror showing asperities of different diameters that produce spatially and thermally variable heat pulses and textures. Note different vertical and horizontal scales. (B) Thermomechanical simulation results showing time–temperature paths for hematite at fault surface ($z = 0$ mm) for flash heating at a 20 μm diameter asperity. Dashed portion of x-axis is schematic pre-slip time interval. Dashed and solid yellow bars beneath x-axis indicate pre- and post-slip periods, respectively. Red portion denotes slip event and associated temperature rise. (C) He loss with depth for diffusion domains of different radius r for 20 μm asperity flash heating scenario. Red shaded region indicates bulk He loss for dominant 0.1–0.5 μm grain radii in most fault surface aliquots. Vertical dashed line denotes typical $\sim$200 μm aliquot thickness. (For interpretation of the references to color in this figure legend, the reader is referred to the web version of this article.)

ening of frictional contacts by asperity flash heating (Rice, 2006; Hirose and Bystricky, 2007; Goldsby and Tullis, 2011). Dynamic weakening typically results in measured friction coefficients of 0.1, in contrast to static, or low slip rate, friction coefficients of $\sim$0.4–0.8 (e.g., Byerlee, 1978; Di Toro et al., 2011). Importantly, frictional weakening during slip is a necessary condition for earthquake rupture propagation (Brace and Byerlee, 1966; Scholz, 1998 and references therein).

We suggest spatially isolated clusters of polygonal and lobate grains at the surface of hematite fault mirrors are the thermal and mechanical footprints of geometric asperities (Fig. 4A). Micro-scale frictional contacts on the fault surface concentrate stress, resulting in localized thermal anomalies or flash heating during rapid fault slip (Fig. 4A; Dieterich and Kilgore, 1994; Rice, 2006). The correlation between high-temperature microtextures and thermally reset hematite He dates suggests this process operated on exhumed WFZ hematite fault mirrors. We further explore this interpretation with a suite of thermomechanical models. These models (1) calculate the temperature evolution through time at frictional contacts on the fault surface and (2) couple these outputs to a model of He loss from hematite. We first discuss the model framework and parameterization followed by simulation results. An abbreviated description of the model setup is presented here. And additional details of our calculations as well as a discussion of thermal history sensitivity to parameter choice are described in the Supplementary Material.

6.1. Model framework and parameterization

The temperature at a frictional contact, T_{fc}, is (Rice, 2006):

$$T_{fc} = T_{surf} + \frac{\mu_{fc} H V \sqrt{\beta}}{\rho C \sqrt{\pi \alpha}} \tag{1}$$

where T_{surf} is the macroscopic (i.e., fault surface-averaged) temperature over the slipping patch, μ_{fc} is the contact coefficient of friction, H is the indentation hardness of the mineral, V is the slip velocity, β is the asperity lifetime (diameter/V), ρ is density, C is heat capacity, and α is thermal diffusivity. The term T_{surf} in equation (1) is derived from Lachenbruch (1986):

$$T_{surf} = \frac{\mu \sigma_n V t^*}{2 \rho C h} + T_{amb} = \frac{\tau D}{2 \rho C h} + T_{amb} \tag{2}$$

where t^* is the duration of slip, T_{amb} is ambient temperature, μ is the coefficient of friction, σ_n is the normal stress, τ is shear stress, and D is displacement.

We calculate the temperature profile beneath and asperity and within the shear zone during and after slip with a 1D thermal model (Lachenbruch, 1986). Temperature, T, is:

$$
\begin{aligned}
T(z,t) &= \frac{\tau V}{2 \rho C h} \left[t \left(1 - 2i^2 \operatorname{erfc} \frac{h-z}{\sqrt{4\alpha t}} - 2i^2 \operatorname{erfc} \frac{h+z}{\sqrt{4\alpha t}} \right) \right. \\
&\quad - (t - t^*) \left(1 - 2i^2 \operatorname{erfc} \frac{h-z}{\sqrt{4\alpha(t-t^*)}} \right. \\
&\quad \left. \left. - 2i^2 \operatorname{erfc} \frac{h+z}{\sqrt{4\alpha(t-t^*)}} \right) \right] + T_{amb}
\end{aligned}
\tag{3}
$$

where z is shear zone depth, t is time, and h is half width of the deforming zone. The term $i^2 \operatorname{erfc}(\delta)$ denotes the second integral of the complementary error function of δ. The time-integrated thermal history as a function of shear zone depth is coupled to a model of He volume diffusion (Fechtig and Kalbitzer, 1966; see Supplementary Material). We posit He loss from hematite crystals during faulting occurs via a combination of recrystallization and thermally activated volume diffusion. Polygonal and lobate hematite crystals interpreted as recrystallization features are isolated in <20 um clusters and rarely extend more than ~10 μm into the underlying comminuted hematite (Fig. S4). He is completely lost from recrystallized regions, but this only affects a volumetrically small portion of our dated aliquots. For simplicity, we calculate He loss by time–temperature-dependent volume diffusion as a proxy for slip-induced He loss regardless of process. Our use of a 1D temperature

model has the implicit assumption that the asperity distribution and spacing across the fault surface was not sparse enough create fault-parallel thermal gradients that substantially exceed the fault-perpendicular gradient (i.e., heat transfer occurs dominantly in one direction). We emphasize that our calculated temperatures reflect the maximum temperatures at any given depth in the shear zone and that the 1D calculation becomes less realistic with increasing distance from the slip surface.

Model simulations set V at 1 m/s, to be consistent with seismic slip rates and evidence for frictional heating on hematite fault mirrors (e.g., Sibson, 1975; Heaton, 1990; Spray, 1992; Rowe and Griffith, 2015 and references therein). We posit that μ_{fc} evolves from 0.6 to 0.1, but is closer to 0.6, over the contact lifetime and thus assume an average μ_{fc} of 0.4. We set $H = 2.7$ GPa, a typical value for hematite (Chicot et al., 2011). The terms ρ, C, α are 2700 kg/m^3, 790 J/kg K, and 1.27×10^{-6} m^2/s, respectively, to be consistent with the typical physical properties of granitic host rock (Robertson, 1988). We select asperity contact diameters consistent with the observed spatial extent of high-temperature microtextures, ~1–20 μm (Figs. 2; S4), although we model contact diameters up to 50 μm. In equation (2), μ is assumed to be 0.1, consistent with the average μ observed in rotary shear experiments conducted at seismic slip rates (e.g., Di Toro et al., 2011; Goldsby and Tullis, 2011), and displacement D and half-width h are assumed to be 6.5 cm and 1 mm, respectively. These two parameter choices reflect the average displacement and shear zone half-width observed in the field. Observed displacement is likely cumulative and this value represents an upper bound on macroscopic shear heating from equation (2). Hematite and apatite He data patterns suggest that slip events occur at depths ≤2 km. Assuming a 30 °C/km geothermal gradient (Blackett, 2004) and lithostatic pressure yields T_{amb} and σ_n of 45 °C and 40 MPa, respectively, at our chosen model depth of 1.5 km. The local coseismic and post-seismic temperature distribution from flash heating at asperities is calculated by equating the total temperature rise from equation (1) to an "equivalent" τ for use in equation (3). He loss is modeled from a range of grain sizes corresponding to our observed grain size distribution and using hematite He diffusion kinetics from Evenson et al. (2014).

6.2. Model results

Thermomechanical simulations indicate flash heating of asperities can generate temperatures required to explain hematite grain morphologies and reset He dates (Fig. 4B). Hematite He dates are most sensitive to the maximum temperature experienced during slip. Peak asperity flash temperature is proportional to contact diameter [equation (1)]. The largest observed diameter of clustered polygonal grains is ~20 μm (Fig. S4) and gives an estimate of the likely peak temperature on these fault mirrors. In this scenario, peak asperity temperature is ~1240 °C (Fig. 4B). He loss occurs from a variety of grain sizes observed in hematite-coated fault surfaces, with ~85–100% fractional loss from domains with radii of 0.1–0.5 μm within 200 μm of the fault surface (typical aliquot thickness; Figs. 4C; S2; S3). Complete resetting occurs for smaller grain radii and plates with 5 and 10 μm half-widths display ~13% and ~7% He loss, respectively (Fig. 4B). Peak slip surface temperatures associated with asperities of 1–50 μm diameters range from 360 to 1900 °C (Fig. 5A) and result in 0–100% He loss from 0.1 μm domains, the lower end of the observed bulk grain size distribution (Fig. 5B). Calculated peak asperity temperatures are not strongly sensitive our choice of T_{surf}, which only contributes a temperature rise above T_{amb} of ~60 °C (Fig. 5A, inset). Reducing displacement so that macroscopic temperature rise is small [i.e., $T_{surf} \approx T_{amb}$ in equation (1)] results in a negligible change to calculated He loss in all simulations.
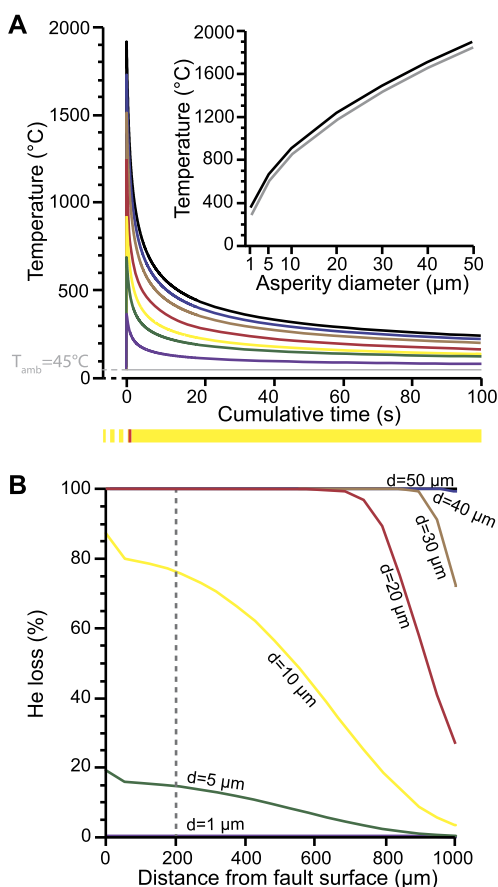
A

B

Fig. 5. (A) Time–temperature histories for asperities of different diameter (d) at the fault surface ($z = 0$ mm). x-Axis annotations are those in Fig. 4A. Inset shows peak asperity temperature as a function of d with (black line) and without (gray line) contribution from 6.5 cm of displacement. (B) He loss with depth from 0.1 μm domain for different asperity d values. Colors correspond to time–temperature curves in (A). Vertical dashed line denotes typical ∼200 μm aliquot thickness. (For interpretation of the references to color in this figure legend, the reader is referred to the web version of this article.)

For comparison to asperity flash heating simulations, we calculate fault surface temperatures and associated He loss from macroscopic, or bulk surface, shear heating [i.e., using equations (2) and (3); Fig. S5]. These simulations vary D (1–10 cm), V (0.1–1 m/s), and average τ (2.7–42.4 MPa). Parameter ranges are further discussed in the Supplementary Material. T_{surf} is ∼105 °C for $D = 6.5$ cm, $V = 1$ m/s, and $\tau = 4$ MPa and yields negligible He loss. Other simulations indicate that He loss (5–100%) can only be achieved for displacements ≥5 cm and at high τ associated with slip at depths equal to or greater than the apatite He T_c isotherm, and/or high coefficients of friction ($\mu = 0.8$). Observed displacements across hematite fault mirrors are typically <10 cm and average 6.5 cm. Multiple generations of slickenlines also indicate that displacement potentially accumulated over multiple slip events, and displacement per event was likely less than even the average estimate. In addition, hematite and apatite He data patterns indicate that many surfaces experience resetting below the apatite He T_c isotherm, where σ_n at the macroscopic scale is insufficient to induce measurable He loss. Effective σ_n will be lower in the presence of fluid pressure, which we do not consider in these simulations.

Thermomechanical simulations reveal our microtextural and thermochronometry data patterns reflect transient, localized thermal pulses (∼>700–1200 °C) from asperity flash heating during fault slip. Peak flash temperatures and temperature distribution in space and time was likely heterogeneous on each analyzed fault

mirror. Bulk hematite He dates reflect thermal resetting from the time-variant activation of a 2D spatial distribution of asperities across aliquots and slip surfaces (Figs. 3C; 4A). Intrasample scatter in hematite He dates from these samples may also reflect (1) the size of all analyzed aliquots exceeds regions impacted by high temperatures, and (2) dated, SEM-prescreened hematite aliquots purposefully encapsulate a range of observed microtextures, not solely polygonal/lobate grains. In addition, the asperity (flash) temperature distribution will control macroscopic scale heating and fault strength (e.g., Rice, 2006; Beeler et al., 2008). Hematite He dates from samples comprising aliquots with a higher volume fraction of polygonal/lobate grains such as W15-16A and W15-16C are comparatively reproducible versus other samples in Fig. 3C. This suggests the asperity distribution, and thus heating, was more uniform across this surface relative to others.

7. Seismicity on hematite fault mirrors

Asperity flash heating and concomitant weakening likely promote earthquakes on these high-gloss fault surfaces. Most rocks experience dramatic strength reduction of micro-contacts at temperatures ≥900–1000 °C (Spray, 1992; Rice, 2006; Goldsby and Tullis, 2011). Inferred paleoasperity dimensions and model simulations parameterized by our data indicate flash-heating temperatures >360–1200 °C (Fig. 5A inset), although measurable He loss by volume diffusion requires temperatures of at least ∼700 °C. Hematite asperity contacts that experienced the upper end of this temperature range may have failed, resulting in dynamic weakening. Our results do not preclude other weakening mechanisms operating on these fault surfaces, but provide compelling evidence that asperity flash heating does occur during slip. Strength reduction during slip is a requirement for earthquake rupture propagation and seismogenic slip. Evidence for frictional heating and dynamic weakening suggests that WFZ hematite fault mirrors accommodated ancient seismicity.

We calculate potential moment magnitudes (M_w) for documented paleoearthquakes (details in Supplementary Material). Exposed hematite-coated fault mirrors crop out in 0.3–30 m^2 isolated patches (Evans and Langrock, 1994; Evans et al., 2014). If these are representative of the original dimensions of ruptured slip patches, seismological scaling relationships (e.g., Kwiatek et al., 2011) indicate 0.3 and 30 m^2 slip patches likely accommodated single-event displacements of ∼10–40 μm and 2–4 mm, respectively. This yields $M_w = -3.4$ to 0.3. The average observed displacement (6.5 cm) likely represents slip accumulated over many events, supported by multiple overprinting slickenline orientations preserved on most surfaces. We calculate an upper bound on M_w assuming that the average displacement reflects a single event. Theoretical relationships between slip and rupture area (Scholz, 2002; see Supplementary Material) indicate 6.5 cm of displacement would be associated with a slip patch of ∼5340 m^2, yielding $M_w = 2.6$. Reasonable M_w estimates for earthquakes accommodated on these fault surfaces are thus ∼−3.4 to 2.6. Following Eaton et al. (2016), seismic events at the lower end of this range of M_w (i.e., $M_w = -3.4$ to 0.3) correspond to nano- to milliseismicity. However, some fault mirrors may have hosted larger seismic events. Hematite and apatite He data patterns constrain the timing and depth of at least some of these earthquakes to post-4.5 Ma and ≤2 km, although earlier slip at greater depths also likely occurred.

We reconstruct the rock record of paleoearthquakes from damage zone slip surfaces that are spatially and temporally correlated with the active, seismogenic Wasatch Fault system. The WFZ has produced ≥ M_w 7 earthquakes every ∼500–2500 yr through the Holocene (DuRoss et al., 2016 and references therein). Small earthquakes on hematite fault mirrors may represent aftershock clouds

in response to larger seismic events. Recent studies suggest smaller earthquakes are self-similar with larger earthquakes and that similar physical processes control the genesis of both (e.g., Ide and Beroza, 2001; Kwiatek et al., 2011). Our data argue that flash heating of asperities is a viable mechanism for generating small earthquakes and we suggest this process may also promote larger seismic events. Consideration of dynamic weakening by asperity flash heating in models of earthquake rupture may inform the genesis and behavior of larger earthquakes along the Wasatch Front and in other fault zones.

8. Conclusions

Integrated microtextural observations, fault rock thermochronometry, and thermomechanical modeling quantify fault surface paleotemperatures and reveal a rock record of seismicity preserved on WFZ hematite fault mirrors. Hematite aliquots with clusters of polygonal and lobate grains that yield He dates younger than apatite He data provide evidence of friction-generated temperatures at the fault surface, hematite recrystallization, and attendant He loss. Transient flash temperatures of >~700–1200 °C at frictional contacts on the slipping surface and subsequent weakening likely enabled seismogenic slip. Hematite and apatite He data patterns constrain some of these events to post-4.5 Ma and at ≤2 km depth. The exhumed damage zone fault mirrors archive thermal and mechanical processes operative along a major normal fault in the western USA during footwall exhumation. Asperity flash heating is hypothesized as a weakening mechanism during earthquake genesis and rupture propagation by laboratory and theoretical studies (e.g., Rice, 2006; Hirose and Bystricky, 2007; Beeler et al., 2008; Goldsby and Tullis, 2011). We provide evidence of this process occurring in a natural, exumed fault damage zone. If our documented weakening process scales with larger seismic events, asperity flash heating may be an important process in the propagation of ruptures associated with larger earthquakes.

Acknowledgements

Appendix A. Supplementary material

Supplementary material related to this article can be found online at http://dx.doi.org/10.1016/j.epsl.2017.04.020.

References

Armstrong, P.A., Taylor, A.R., Ehlers, T.A., 2004. Is the Wasatch fault footwall (Utah, United States) segmented over million-year time scales? Geology 32, 385–388.

Ault, A.K., Frenzel, M., Reiners, P.W., Woodcock, N.H., Thomson, S.N., 2016. Record of paleofluid circulation in faults revealed by hematite (U–Th)/He and apatite fission-track dating: an example from Gower Peninsula fault fissures, Wales. Lithosphere 8 (4), 379–385.

Ault, A.K., Reiners, P.W., Evans, J.P., Thomson, S.N., 2015. Linking hematite (U–Th)/He dating with the microtextural record of seismicity in the Wasatch fault damage zone, Utah, USA. Geology 43, 771–774.

Beeler, N., Tullis, T., Goldsby, D., 2008. Constitutive relationships and physical basis of fault strength due to flash heating. J. Geophys. Res., Solid Earth 113.

Blackett, R.E., 2004. Geothermal gradient data for Utah. Trans., Geotherm. Resour. Counc. 28, 3–6.

Brace, W., Byerlee, J., 1966. Stick-slip as a mechanism for earthquakes. Science 153, 990–992.

Brantut, N., Schubnel, A., Rouzaud, J.N., Brunet, F., Shimamoto, T., 2008. High-velocity frictional properties of a clay-bearing fault gouge and implications for earthquake mechanics. J. Geophys. Res., Solid Earth 113, B01401.

Byerlee, J., 1978. Friction of rocks. Pure Appl. Geophys. 116, 615–626.

Chicot, D., Mendoza, J., Zaoui, A., Louis, G., Lepingle, V., Roudet, F., Lesage, J., 2011. Mechanical properties of magnetite (Fe_3O_4), hematite (α-Fe_2O_3) and goethite (α-FeOOH) by instrumented indentation and molecular dynamics analysis. Mater. Chem. Phys. 129, 862–870.

Collettini, C., Viti, C., Tesei, T., Mollo, S., 2013. Thermal decomposition along natural carbonate faults during earthquakes. Geology 41, 927–930.

De Paola, N., Holdsworth, R.E., Viti, C., Collettini, C., Bullock, R., 2015. Can grain size sensitive flow lubricate faults during the initial stages of earthquake propagation? Earth Planet. Sci. Lett. 431, 48–58.

Di Toro, G., Han, R., Hirose, T., De Paola, N., Nielsen, S., Mizoguchi, K., Ferri, F., Cocco, M., Shimamoto, T., 2011. Fault lubrication during earthquakes. Nature 471, 494–498.

Dieterich, J.H., 1979. Modeling of rock friction, 1: experimental results and constitutive equations. J. Geophys. Res., Solid Earth 84, 2161–2168.

Dieterich, J.H., Kilgore, B.D., 1994. Direct observation of frictional contacts: new insights for state-dependent properties. Pure Appl. Geophys. 143, 283–302.

Dieterich, J.H., Kilgore, B., 1996. Implications of fault constitutive properties for earthquake prediction. Proc. Natl. Acad. Sci. USA 93, 3787–3794.

Dodson, M.H., 1973. Closure temperature in cooling geochronological and petrological systems. Contrib. Mineral. Petrol. 40, 259–274.

DuRoss, C.B., Personius, S.F., Crone, A.J., Olig, S.S., Hylland, M.D., Lund, W.R., Schwartz, D.P., 2016. Fault segmentation: new concepts from the Wasatch Fault Zone, Utah, USA. J. Geophys. Res., Solid Earth.

Eaton, D.W., van der Baan, M., Ingelson, A., 2016. Terminology for fluid-injection induced seismicity in oil and gas operations. Recorder 41, 5.

Ehlers, T.A., Willett, S.D., Armstrong, P.A., Chapman, D.S., 2003. Exhumation of the central Wasatch Mountains, Utah, 2: thermokinematic model of exhumation, erosion, and thermochronometer interpretation. J. Geophys. Res., Solid Earth 108.

Evans, J.P., Langrock, H., 1994. Structural analysis of the Brigham City–Weber segment boundary zone, Wasatch normal fault, Utah: implications for fault growth and structure. Pure Appl. Geophys. 142, 663–685.

Evans, J.P., Prante, M.R., Janecke, S.U., Ault, A.K., Newell, D.L., 2014. Hot faults: iridescent slip surfaces with metallic luster document high-temperature ancient seismicity in the Wasatch fault zone, Utah, USA. Geology 42, 623–626.

Evenson, N.S., Reiners, P.W., Spencer, J.E., Shuster, D.L., 2014. Hematite and Mn oxide (U–Th)/He dates from the Buckskin–Rawhide detachment system, western Arizona: gaining insights into hematite (U–Th)/He systematics. Am. J. Sci. 314, 1373–1435.

Farley, K., Flowers, R., 2012. (U–Th)/Ne and multidomain (U–Th)/He systematics of a hydrothermal hematite from eastern Grand Canyon. Earth Planet. Sci. Lett. 359, 131–140.

Fechtig, H., Kalbitzer, S., 1966. The diffusion of argon in potassium-bearing solids. In: Potassium Argon Dating. Springer, pp. 68–107.

Flowers, R.M., Ketcham, R.A., Shuster, D.L., Farley, K.A., 2009. Apatite (U–Th)/He thermochronometry using a radiation damage accumulation and annealing model. Geochim. Cosmochim. Acta 73, 2347–2365.

Goldsby, D.L., Tullis, T.E., 2011. Flash heating leads to low frictional strength of crustal rocks at earthquake slip rates. Science 334, 216–218.

Heaton, T.H., 1990. Evidence for and implications of self-healing pulses of slip in earthquake rupture. Phys. Earth Planet. Inter. 64, 1–20.

Hirose, T., Bystricky, M., 2007. Extreme dynamic weakening of faults during dehydration by coseismic shear heating. Geophys. Res. Lett. 34 (14), L14311.

Hirose, T., Shimamoto, T., 2005. Growth of molten zone as a mechanism of slip weakening of simulated faults in gabbro during frictional melting. J. Geophys. Res., Solid Earth 110, B05202.

Ide, S., Beroza, G.C., 2001. Does apparent stress vary with earthquake size? Geophys. Res. Lett. 28, 3349–3352.

Kanamori, H., Rivera, L., 2006. Energy partitioning during an earthquake. In: Earthquakes: Radiated Energy and the Physics of Faulting, pp. 3–13.

Kirkpatrick, J., Rowe, C., White, J., Brodsky, E., 2013. Silica gel formation during fault slip: evidence from the rock record. Geology 41, 1015–1018.

Kwiatek, G., Plenkers, K., Dresen, G., Group, J.R., 2011. Source parameters of picoseismicity recorded at Mponeng deep gold mine, South Africa: implications for scaling relations. Bull. Seismol. Soc. Am. 101, 2592–2608.

Lachenbruch, A.H., 1986. Simple Models for the Estimation and Measurement of Frictional Heating by an Earthquake. US Geological Survey.

Lapusta, N., Rice, J.R., 2003. Nucleation and early seismic propagation of small and large events in a crustal earthquake model. J. Geophys. Res., Solid Earth 108, 2205.

Polissar, P.J., Savage, H.M., Brodsky, E.E., 2011. Extractable organic material in fault zones as a tool to investigate frictional stress. Earth Planet. Sci. Lett. 311, 439–447.

Reiners, P.W., 2009. Nonmonotonic thermal histories and contrasting kinetics of multiple thermochronometers. Geochim. Cosmochim. Acta 73, 3612–3629.

Rice, J.R., 2006. Heating and weakening of faults during earthquake slip. J. Geophys. Res., Solid Earth 111.

Robertson, E.C., 1988. Thermal Properties of Rocks. US Geological Survey.

Rowe, C.D., Griffith, W.A., 2015. Do faults preserve a record of seismic slip: a second opinion. J. Struct. Geol. 78, 1–26.

Scholz, C.H., 1998. Earthquakes and friction laws. Nature 391, 37–42.

Scholz, C.H., 2002. The Mechanics of Earthquakes and Faulting. Cambridge University Press.

Sibson, R.H., 1975. Generation of pseudotachylyte by ancient seismic faulting. Geophys. J. Int. 43, 775–794.

Siemes, H., Klingenberg, B., Rybacki, E., Naumann, M., Schäfer, W., Jansen, E., Rosière, C.A., 2003. Texture, microstructure, and strength of hematite ores experimentally deformed in the temperature range 600–1100 °C and at strain rates between 10^{-4} and 10^{-6} s^{-1}. J. Struct. Geol. 25, 1371–1391.

Siemes, H., Rybacki, E., Klingenberg, B., Rosière, C.A., 2011. Development of a recrystallized grain size piezometer for hematite based on high-temperature torsion experiments. Eur. J. Mineral. 23, 293–302.

Smith, S., Di Toro, G., Kim, S., Ree, J.-H., Nielsen, S., Billi, A., Spiess, R., 2013. Coseismic recrystallization during shallow earthquake slip. Geology 41, 63–66.

Spray, J.G., 1992. A physical basis for the frictional melting of some rock-forming minerals. Tectonophysics 204, 205–221.

Trepmann, C.A., Stöckhert, B., Dorner, D., Moghadam, R.H., Küster, M., Röller, K., 2007. Simulating coseismic deformation of quartz in the middle crust and fabric evolution during postseismic stress relaxation—an experimental study. Tectonophysics 442, 83–104.

Vallina, B., Rodriguez-Blanco, J.D., Brown, A., Benning, L., Blanco, J., 2014. Enhanced magnetic coercivity of α-Fe$_2$O$_3$ obtained from carbonated 2-line ferrihydrite. J. Nanopart. Res. 16, 1–13.

Zheng, G., Rice, J.R., 1998. Conditions under which velocity-weakening friction allows a self-healing versus a cracklike mode of rupture. Bull. Seismol. Soc. Am. 88, 1466–1483.